ISPRS Journal of Photogrammetry and Remote Sensing xxx (2015) xxx–xxx

Contents lists available at ScienceDirect

ISPRS Journal of Photogrammetry and Remote Sensing

journal homepage: www.elsevier.com/locate/isprsjprs

Review Article

Persistent Scatterer Interferometry: A review

Michele Crosetto [a,*], Oriol Monserrat [a], María Cuevas-González [a], Núria Devanthéry [a], Bruno Crippa [b]

[a] Centre Tecnològic de Telecomunicacions de Catalunya (CTTC), Division of Geomatics, Av. Gauss 7, E-08860 Castelldefels, Barcelona, Spain
[b] Department of Earth Sciences, University of Milan, Via Cicognara 7, I-20129 Milan, Italy

ARTICLE INFO

Article history:
Received 13 May 2015
Received in revised form 26 October 2015
Accepted 28 October 2015
Available online xxxx

Keywords:
Remote sensing
Radar
SAR
Monitoring
Deformation

ABSTRACT

Persistent Scatterer Interferometry (PSI) is a powerful remote sensing technique able to measure and monitor displacements of the Earth's surface over time. Specifically, PSI is a radar-based technique that belongs to the group of differential interferometric Synthetic Aperture Radar (SAR). This paper provides a review of such PSI technique. It firstly recalls the basic principles of SAR interferometry, differential SAR interferometry and PSI. Then, a review of the main PSI algorithms proposed in the literature is provided, describing the main approaches and the most important works devoted to single aspects of PSI. A central part of this paper is devoted to the discussion of different characteristics and technical aspects of PSI, e.g. SAR data availability, maximum deformation rates, deformation time series, thermal expansion component of PSI observations, etc. The paper then goes through the most important PSI validation activities, which have provided valuable inputs for the PSI development and its acceptability at scientific, technical and commercial level. This is followed by a description of the main PSI applications developed in the last fifteen years. The paper concludes with a discussion of the main open PSI problems and the associated future research lines.

1. Introduction

This paper offers a review of Persistent Scatterer Interferometry (PSI), a powerful remote sensing technique able to measure displacements of the Earth's surface. In this work, the terms displacement and deformation are used interchangeably. As it is later described in more detail, PSI represents a specific class of the Differential Interferometric Synthetic Aperture Radar (DInSAR) techniques. Such techniques exploit the information contained in the radar phase of at least two complex SAR images acquired in different times over the same area, which are used to form an interferometric pair. The repeated acquisition of images over a given area is usually performed with the same sensor or sensors with identical system characteristics. Gabriel et al. (1989) provided the first description of DInSAR, which was based on L-band Seasat data. For a general review of SAR interferometry, see Bamler and Hartl (1998) and Rosen et al. (2000).

The DInSAR principle is briefly summarized below. Considering a single pixel footprint on the ground P, the sensor acquires a first SAR image from a satellite position M, measuring a phase φ_M:

$$\varphi_M = \varphi_{geom\text{-}M} + \varphi_{scatt\text{-}M} = \frac{4 \cdot \pi \cdot MP}{\lambda} + \varphi_{scatt\text{-}M} \quad (1)$$

where MP is the sensor to target distance, φ_{scatt} is the phase shift generated during the interaction between the microwaves and the target P, λ is the radar wavelength, and the factor 4π is related to the two way path, radar-target-radar. Assuming that the sensor acquires a second image from a satellite position S, measuring the phase φ_S over the same pixel footprint P, then:

$$\varphi_S = \varphi_{geom\text{-}S} + \varphi_{scatt\text{-}S} = \frac{4 \cdot \pi \cdot SP}{\lambda} + \varphi_{scatt\text{-}S} \quad (2)$$

The Interferometric SAR (InSAR) technique exploits the phase difference $\varphi_S - \varphi_M$:

$$\Delta\varphi_{Int} = \varphi_S - \varphi_M = \frac{SP - MP}{\frac{\lambda}{4 \cdot \pi}} + \varphi_{scatt\text{-}S} - \varphi_{scatt\text{-}M} \quad (3)$$

This phase is called interferometric phase and is related to the distance difference $SP - MP$, which is fundamental for Digital Elevation Model (DEM) generation, i.e. to estimate the topography of the observed scene, see Bamler and Hartl (1998) and Rosen

* Corresponding author.
E-mail addresses: mcrosetto@cttc.cat (M. Crosetto), omonserrat@cttc.cat (O. Monserrat), mcuevas@cttc.cat (M. Cuevas-González), ndevanthery@cttc.cat (N. Devanthéry), bruno.crippa@unimi.it (B. Crippa).

http://dx.doi.org/10.1016/j.isprsjprs.2015.10.011
0924-2716/

et al. (2000). The InSAR sensitivity to topography depends on the satellite baseline *SM*, and more specifically on the projection of *SM* in the direction perpendicular to the SAR Line-Of-Sight (LOS), called perpendicular baseline. In the case of DInSAR deformation measurement, considering a single pixel footprint P and a first acquisition from the satellite position *M* (see Fig. 1), a phase φ_M is measured, see Eq. (1). Then, assuming that the target moves from P to P′ and that, afterwards, the sensor acquires a second image from the satellite position *S*, φ_S is estimated:

$$\varphi_S = \varphi_{geom\text{-}S} + \varphi_{scatt\text{-}S} = \frac{4 \cdot \pi \cdot SP'}{\lambda} + \varphi_{scatt\text{-}S} \tag{4}$$

In this case, the interferometric phase $\Delta\varphi_{Int}$ is given by:

$$\Delta\varphi_{Int} = \varphi_S - \varphi_M = \frac{SP' - MP}{\frac{\lambda}{4\cdot\pi}} + \varphi_{scatt\text{-}S} - \varphi_{scatt\text{-}M} \tag{5}$$

By adding and subtracting the term $SP/(\frac{\lambda}{4\cdot\pi})$ the following equation is obtained:

$$\Delta\varphi_{Int} = \varphi_S - \varphi_M = \frac{SP - MP}{\frac{\lambda}{4\cdot\pi}} + \frac{SP' - SP}{\frac{\lambda}{4\cdot\pi}} + \varphi_{scatt\text{-}S} - \varphi_{scatt\text{-}M} \tag{6}$$

where the first term is the topographic phase component φ_{Topo}, which includes the so-called reference ellipsoidal phase component, and the second term is the displacement phase component φ_{Displ}, related to the LOS displacement d shown in Fig. 1. Assuming that the last two terms of Eq. (6) cancel out, if a DEM of the imaged scene is available, φ_{Topo} can be simulated and subtracted from $\Delta\varphi_{Int}$ (this is the inverse operation performed in InSAR DEM generation), obtaining the so-called DInSAR phase $\Delta\varphi_{D\text{-}Int}$:

$$\Delta\varphi_{D\text{-}Int} = \Delta\varphi_{Int} - \varphi_{Topo\_simu} = \varphi_{Displ} \tag{7}$$

where φ_{Topo_simu} is the simulated topographic component, which implicitly contains flat-earth phase component. Note that the orbital errors affect this simulated topographic component, even if the flattening process is not explicitly done. Eq. (7) summarizes the DInSAR working principle, which allows the displacements of the imaged scene to be derived from two complex SAR images. This principle has been widely exploited in the last 25 years, yielding significant results in the fields of seismology (Massonnet et al., 1993; Peltzer and Rosen, 1995; Dalla Via et al., 2012), vulcanology (Massonnet et al., 1995; Massonnet and Sigmundsson, 2000; Antonielli et al., 2014), glaciology (Goldstein et al., 1993; Rignot et al., 1997), landslides (Carnec et al., 1996; García-Davalillo et al., 2014), ground subsidence and uplift (Galloway et al., 1998; Amelung et al., 1999), etc. Comprehensive reviews of different DInSAR applications are provided by Massonnet and Feigl (1998) and Hanssen (2001).

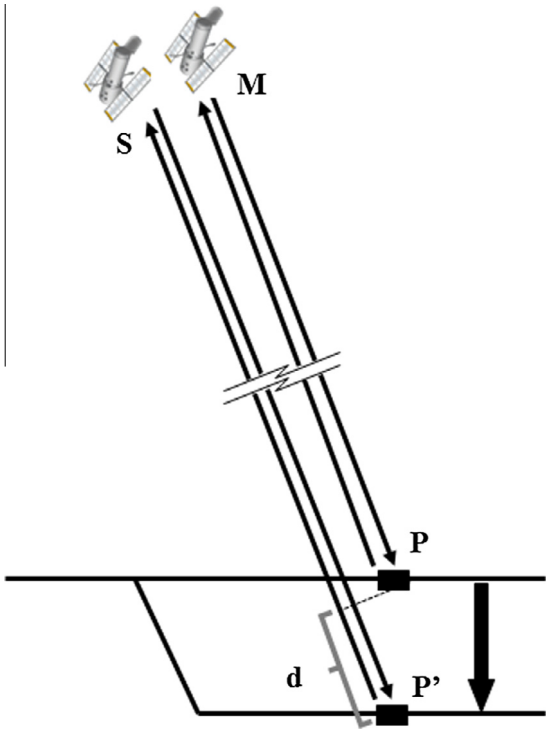

Fig. 1. Scheme of the DInSAR deformation measurement.

Eq. (7) represents a simplified DInSAR observation equation. A comprehensive equation includes:

$$\Delta\varphi_{D-Int} = \Delta\varphi_{Int} - \varphi_{Topo\_simu} = \varphi_{Displ} + \varphi_{Topo\_res} + \varphi_{Atm\_S} - \varphi_{Atm\_M} + \varphi_{Orb\_S} - \varphi_{Orb\_M} + \varphi_{Noise} + 2 \cdot k \cdot \pi \tag{8}$$

where φ_{Topo_res} is the residual topographic error (RTE) component, φ_{Atm} is the atmospheric phase component at the time of acquisition of each image, φ_{Orb} is the phase component due to the orbital errors of each image (errors that affect the position of *M* and *S* in Fig. 1) and φ_{Noise} is the phase noise. The last term, $2 \cdot k \cdot \pi$, where *k* is an integer value called phase ambiguity, is a result of the wrapped nature of $\Delta\varphi_{D\text{-}Int}$, i.e. the fact that the DInSAR phases are bounded in the range $(-\pi, \pi]$.

The goal of any DInSAR technique is to derive φ_{Displ} from $\Delta\varphi_{D-Int}$. This implies separating φ_{Displ} from the other phase components of Eq. (8). An essential condition to accomplish this separation is to analyse pixels characterized by small φ_{Noise}, which are typically related to two types of reflectors: those where the response to the radar is dominated by a strong reflecting object and is constant over time (Permanent Scatterer, PS) and those where the response is constant over time, but is due to different small scattering objects (Distributed Scatterers, DS). The major DInSAR limitations include: (i) the temporal and geometric decorrelations that influence the φ_{Noise} component (Hanssen, 2001); (ii) the phase unwrapping that concerns the estimation of *k* (Ghiglia and Pritt, 1998); and (iii) the atmospheric component (Zebker et al., 1997). The DInSAR stacking techniques (Zebker et al., 1997; Sandwell and Price, 1998; Wright et al., 2001) include different approaches to reduce the atmospheric effects by averaging various interferograms.

PSI represents a specific class of DInSAR techniques, which exploits multiple SAR images acquired over the same area, and appropriate data processing and analysis procedures to separate φ_{Displ} from the other phase components represented in Eq. (8). The term PSI is used in this work to indicate a number of different techniques including the Permanent Scatterers approach (the first PSI technique proposed by Ferretti et al. (2000, 2001)), other techniques based on PSs, those based on DSs and other hybrid methods. Other authors refer to PSI with the terms time series radar interferometry (van Leijen, 2014), advanced DInSAR (Herrera et al., 2007), etc. The main outcomes of a PSI analysis include the deformation time series and the deformation velocity estimated over the analysed PSs or DSs, see an example in Fig. 2. The term PSs will comprise both PSs and DSs hereafter. Another outcome of a PSI analysis is the so-called residual topographic error (RTE), which is the difference between the true height of the scattering phase centre of a given PS and the height of the DEM in this point. The RTE is a key parameter in order to achieve an accurate PS geocoding.

This review considers neither SAR tomography (Reigber and Moreira, 2000; Lombardini, 2005) nor ground-based SAR interferometry (Monserrat et al., 2014) and is organized as follows: the

Please cite this article in press as: Crosetto, M., et al. Persistent Scatterer Interferometry: A review. ISPRS J. Photogram. Remote Sensing (2015), http://dx.doi.org/10.1016/j.isprsjprs.2015.10.011

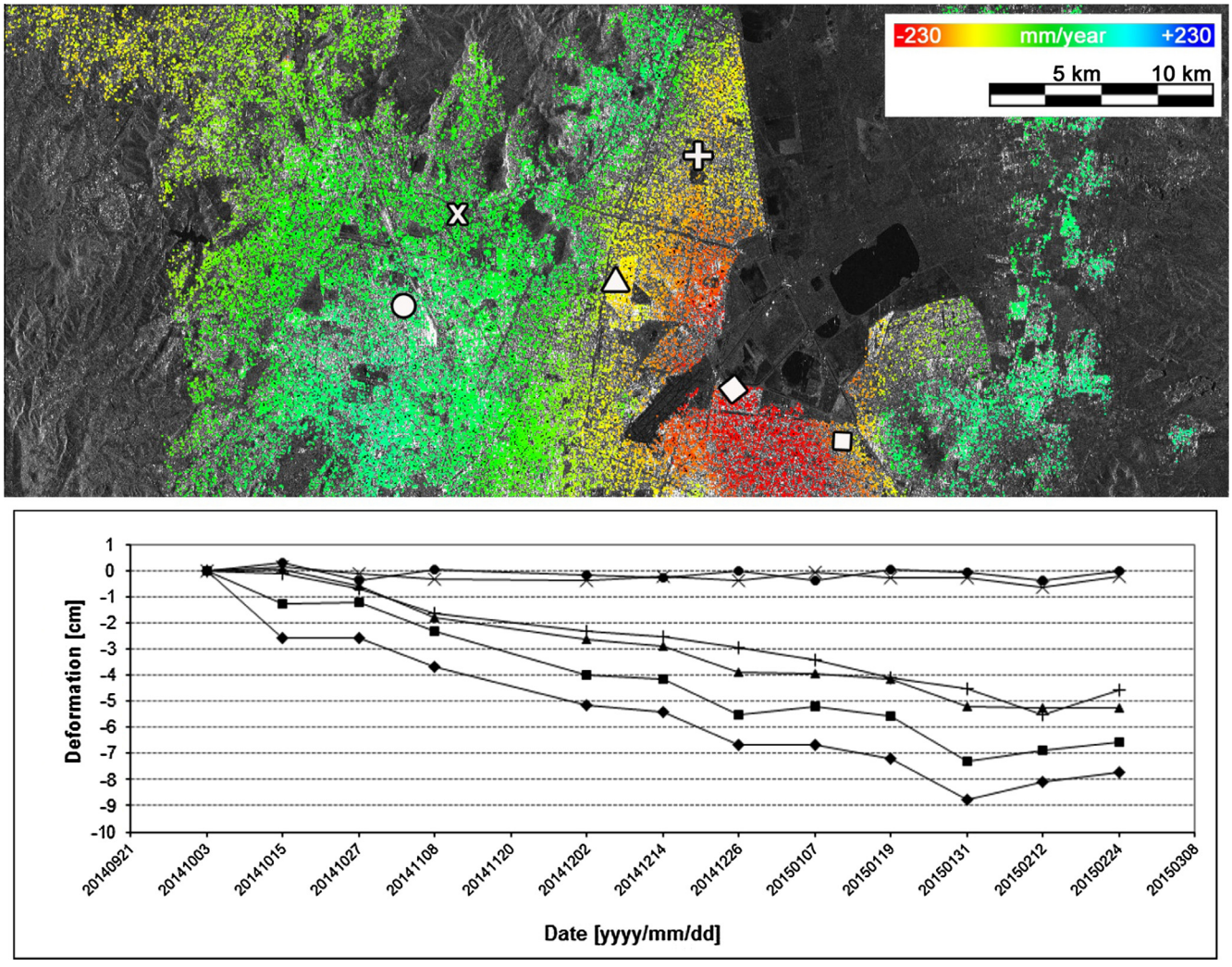

Fig. 2. Example of deformation velocity map and deformation time series estimated using 12 Interferometric Wide Swath SAR Sentinel-1 images over Mexico City.

main PSI algorithms proposed in the literature are examined in Section 2; several technical aspects of the PSI techniques are discussed in Section 3; the validation of the PSI results is described in Section 4; the main PSI applications are reviewed in Section 5; and finally in Section 6 are discussed the main open PSI problems and the associated future research lines.

2. PSI algorithms

In this section, the main PSI algorithms proposed in the literature are discussed. The PSI approaches are firstly described in chronological order. Some of their key characteristics are summarized in Table 1. Four of the most important PSI approaches are then described and discussed in detail. This is then followed by a brief review of the most important works devoted to single aspects of PSI.

The first PSI technique is the Permanent Scatterers approach proposed by Ferretti et al. (2000, 2001). These two publications were preceded by a patent of the PSInSAR™ algorithm and the foundation of a spin-off company by the Politecnico di Milano called Tele-Rilevamento Europa, TRE (www.treuropa.com). These two pioneering works were then followed by several other contributions. The Small BAseline Subset (SBAS) technique (Berardino et al., 2002) is one of the most extensively used. An overview of the SBAS algorithm is provided by Lanari et al. (2007a). Similar approaches to SBAS, based on multilook imagery, were proposed by Mora et al. (2003) and Schmidt and Bürgmann (2003). The same year, two companies specialized in PSI, Gamma Remote Sensing (www.gamma-rs.ch) and Altamira Information (www.altamira-information.com), described their approaches in Werner et al. (2003) and Duro et al. (2003), respectively. Kampes and Hanssen (2004) adapted the LAMBDA method used in GPS to PSI, which was then included in the Spatio-Temporal Unwrapping Network, STUN, described in Kampes (2006). Hooper et al. (2004) described a PSI procedure devoted to analyse episodic crustal deformation in non-urban environments. Crosetto et al. (2005) described a simplified PSI approach based on stepwise linear deformation functions and least squares adjustment. Costantini et al. (2008), see also Costantini et al. (2014), proposed a PSI method that only exploits the relative properties of neighbouring pairs of PSs. López-Quiroz et al. (2009) introduced a new SBAS algorithm based on a temporally parameterized inversion. Ferretti et al. (2011) proposed an extension of the PSInSAR™ algorithm called the SqueeSAR™ algorithm. Perissin and Wang (2012) introduced a PSI approach to exploit partially coherent targets. An algorithm based on wavelet decomposition in space and general parameterization in time was proposed by Hetland et al. (2012). A PSI algorithm based on geodetic estimation theory was proposed by van Leijen (2014). Goel and Adam (2014) described a PSI approach to monitor known

Please cite this article in press as: Crosetto, M., et al. Persistent Scatterer Interferometry: A review. ISPRS J. Photogram. Remote Sensing (2015), http://dx.doi.org/10.1016/j.isprsjprs.2015.10.011

Table 1
Characteristics of the main PSI approaches.

PSI method reference	Baseline configuration	Pixel selection criterion	Deformation model
Ferretti et al. (2000, 2001)	Single master	Amplitude dispersion	Linear deformation in time
Berardino et al. (2002)	Small baselines	Coherence	Spatial smoothness
Mora et al. (2003)	Small baselines	Coherence	Linear deformation in time
Schmidt and Bürgmann (2003)	Small baselines	Coherence	Spatial and temporal smoothness
Werner et al. (2003)	Single master	Amplitude dispersion & Spectral phase diversity	Linear deformation in time
Duro et al. (2003) and Crosetto et al. (2008)	Small baselines	Amplitude dispersion, coherence, spectral coherence	Linear deformation in time
Kampes (2006)	Single master	Amplitude dispersion & Signal to clutter ratio	Different types of deformation models
Hooper et al. (2004)	Single master	Amplitude and phase criterion	Spatial smoothness
Crosetto et al. (2005)	Small baselines	Coherence	Stepwise linear function in time
Costantini et al. (2008)	Single master	Amplitude dispersion	Linear deformation in time
López-Quiroz et al. (2009)	Small baselines	Coherence	Spatial smoothness
Ferretti et al. (2011)	Single master after triangulation	Statistical homogeneity test	Deformation model in time
Perissin and Wang (2012)	Target-dependent interferogram subset	Quasi-PS approach	Linear deformation in time
Hetland et al. (2012)	Small baselines	Coherence	Different types of deformation models
van Leijen (2014)	Single master	Amplitude dispersion	Different types of deformation models
Goel and Adam (2014)	Small baselines	Statistical homogeneity test	Linear deformation in time
Lv et al. (2014)	Single master	Statistical homogeneity test	Linear deformation in time
Devanthéry et al. (2014)	Small baselines	Amplitude dispersion & Cousin PS	Spatial smoothness

surface deformation phenomena, i.e. phenomena whose deformation pattern is known. A PSI approach that exploits the coherence information of neighbouring pixel stacks was proposed by Lv et al. (2014). Finally, Devanthéry et al. (2014) proposed a PSI approach based on the so-called Cousin PSs, which includes a 2 + 1D phase unwrapping algorithm. The main characteristics of the PSI approaches previously mentioned are summarized in Table 1. The baseline configuration, the pixel selection criterion and the used deformation model of each approach are provided. For an extensive review of several PSI techniques see van Leijen (2014).

Four of the most important approaches in terms of impact on the PSI field are concisely discussed below. The PSInSAR™ technique proposed by Ferretti et al. (2000, 2001) is surely the most important one since it represented the first complete solution to select PSs, overcoming the temporal and the geometrical decorrelation, and to estimate deformation and RTE, separating them from the APS contribution. This represented a major step forward with respect to the pre-existing DInSAR techniques, which increased dramatically their applicability and it was a seminal work that provided a basis for further development. The major constraint of this approach is that it is limited to the scatterers that exhibit sufficiently high coherence, even at large baselines, which typically leads to low PS density in nonurban areas. The SBAS technique (Berardino et al., 2002) represents another seminal work that proposes a complete PSI procedure using small baselines to limit the spatial decorrelation, multilooked data to reduce phase noise and a coherence based selection criterion. In addition, it uses an approach to link multiple small baseline subsets. This results in an increased spatial and temporal sampling with respect to the original PSInSAR™ approach. The original SBAS works with multilook imagery and is not suitable for detecting local deformation. This aspect was resolved in an extended SBAS version that works with full-resolution data (Lanari et al., 2004a). Another important PSI contribution was given by Hooper et al. (2004). They proposed a novel PS selection using phase characteristics, which is suitable to find low-amplitude natural targets with phase stability that cannot be identified by amplitude-based algorithms. An important advantage is that it does not require a prior deformation model. This work originated one of the most widely used PSI software packages, StaMPS (Hooper and Zebker, 2007; Hooper, 2008). Finally, a major step forward in PSI is related to the SqueeSAR™ algorithm proposed by Ferretti et al. (2011). They extended the PSInSAR™ algorithm by jointly processing PSs and DSs, taking into account their statistical behaviour. The SqueeSAR™ algorithm is focused on pixels belonging to areas of moderate coherence, where neighbouring pixels share the same reflectivity values as they belong to the same object. The result of SqueeSAR™ is an improved density and quality of the PSI results, which is particularly remarkable in nonurban areas. Other approaches were developed following similar approaches, e.g. see Goel and Adam (2014) and Lv et al. (2014).

Several papers have been devoted to single aspects of PSI and a selection of the most important ones is mentioned here. Perissin and Ferretti (2007) and Dheenathayalan et al. (2011) studied the physical nature of SAR PSs, providing a method to identify and characterize them. van Leijen and Hanssen (2007) described the use of adaptive deformation models to increase PS density. Colesanti et al. (2003) proposed an extension of the PSInSAR™ to monitor seasonal ground deformation phenomena. A similar approach was then used to model the displacements caused by thermal expansion, e.g. see Gernhardt et al. (2010). A more accurate model for thermal expansion is described in Monserrat et al. (2011). Phase unwrapping is one of the most critical processing steps of the PSI techniques. An important topic, addressed by several authors, is the exploitation of the 3D spatio-temporal nature of phase unwrapping of stacks of interferograms, e.g. see Costantini et al. (2002), Pepe and Lanari (2006), Hooper and Zebker (2007), Pepe et al. (2011), Fornaro et al. (2011) and Devanthéry et al. (2014). In general, the 3D phase unwrapping approaches provide better quality results with respect to the 2D interferogram-wise approaches.

The estimation of the atmospheric phase component from PSI observations is another key aspect of the PSI research and Hanssen (2001) provides a detailed analysis of such component. Different methods to correct this atmospheric component have been proposed, including some that use GNSS observations or data from numerical weather models, see Leighton (2010), Catalao et al. (2011), Liu (2012), Jung et al. (2014), Fornaro et al. (2014), Alshawaf et al. (2015), etc.

Several works have been devoted to polarimetric PSI, whose objective is to maximize the quality and number of PSs selected

Please cite this article in press as: Crosetto, M., et al. Persistent Scatterer Interferometry: A review. ISPRS J. Photogram. Remote Sensing (2015), http://dx.doi.org/10.1016/j.isprsjprs.2015.10.011

as reliable a priori by optimizing the parameters used as selection criterion, see Samsonov and Tiampo (2011), Navarro-Sanchez and Lopez-Sanchez (2012, 2014), Navarro-Sanchez et al. (2014). Adam et al. (2011, 2013) described the technical challenges and algorithmic solutions required to extend the PSI mapping from urban areas, where PSI usually shows a good performance, to rural and mountainous regions, thus covering wide areas. Other works related to wide-area PSI include Caro Cuenca et al. (2011) and Costantini et al. (2012). Although most of the PSI results published in the literature were derived using SAR data acquired in StripMap mode, several authors addressed the potentials of different acquisition modes for SAR interferometry and PSI. The differences between the interferometric processing of StripMap and Spotlight SAR data are described in Eineder et al. (2009) and various works have been devoted to the study of the characteristics of the TOPS SAR data acquired by Sentinel-1 (Torres et al., 2012; Rucci et al., 2012). Most of these works have been focused on the TOPS image co-registration, which represents the most critical issue from the interferometric point of view, see De Zan and Monti Guarnieri (2006) and Prats-Iraola et al. (2012). To conclude, it is worth mentioning that there are several open-source DInSAR and PSI analysis tools, see Kampes et al. (2003), Rosen et al. (2004, 2001), Hooper (2008), Sandwell et al. (2011) and Agram et al. (2013). Besides, Perissin et al. (2011) described a software that, although is not open source, is available for collaborative projects.

3. Technical issues

In this section, several characteristics and technical aspects that are particularly relevant from the PSI application point of view are discussed.

3.1. SAR data availability

The capability to sample deformation phenomena over time depends on the availability of SAR data, which in turn depends on the availability of the operating SAR sensors, the SAR satellite revisiting time (the time elapsed between interferometric observations of the area same by a sensor or sensors with identical characteristics), the data acquisition policy, the orbital tube, i.e. the allowed perpendicular baselines (Rocca, 2004), etc. At the time of writing this review, there are several active SAR missions: the four-satellite CosmoSkyMed constellation (X-band), TerraSAR-X and TanDEM-X (X-band), Sentinel-1 (C-band), Radarsat-2 (C-band) and ALOS-2 (L-band). However, the policy on data acquisition of these missions, e.g. background missions (the regular acquisition over given areas) vs. on-demand acquisitions, influences the data availability, which is strongly uneven around the globe. PSI requires a large number of SAR scenes acquired over the same area. Typically, a minimum of 15–20 images is needed to perform a C-band PSI analysis. It is possible to use shorter datasets with X-band PSI due to the higher resolution and the shorter wavelength of this band (Bovenga et al., 2012). Anyhow, the larger the number of available scenes the better the quality of the PSI deformation velocity and time series estimation. Besides, this number is critical for the estimability of those PSI models that involve multiple unknown parameters, e.g. see Monserrat et al. (2011) and van Leijen (2014).

3.2. PS availability

PSI is an opportunistic deformation measurement method, i.e. it is able to measure deformation only over the available PSs. The PS density is usually low in vegetated, forested and low-reflectivity areas (e.g. very smooth surfaces), and in steep terrains facing the radar sensors. Snow coverage, constructions works, street re-pavement, etc. can cause the complete or partial loss of PSs. By contrast, PSs are usually abundant on buildings, monuments, antennas, poles, conducts, exposed rocks or outcrops, among others. Some works have been devoted to the exploitation of temporary or partially coherent PSs, i.e. scatterers that behave as PSs during just a portion of the given data-stack, e.g. see Basilico et al. (2004), Zhang et al. (2011) and Perissin and Wang (2012). The exploitation of such PSs increases remarkably the deformation measurements. Generally, PS location cannot be known before performing the PSI analysis. This can be critical for the study of areas and objects of small spatial extent, because they can be undersampled or even not sampled at all. This aspect is partially mitigated by using X-band very high resolution SAR data (Crosetto et al., 2010). A comparison of the PS density attained using C-band and X-band PSI is shown in Fig. 3. A crucial point of PSI is the difficulty to accurately assign a given PS to an object or a part of an object, unless corner reflectors are used. This is a limiting factor, especially for localized deformation analyses. Interesting works to improve the understanding and interpretation of PSs are Auer et al. (2010, 2011). Regarding the interpretation of the PSI results, there is a remarkable difference between the deformation sampling achievable with PSI and with geodetic and surveying techniques. The latter ones use strategically located points, i.e. points chosen ad hoc to properly sample a given deformation phenomenon. By contrast, PSI performs an opportunistic sampling based on those scatterers that provide a consistent radar reflectance over time. Therefore, the relation between the deformation of those scatterers and the deformation phenomenon of interest has to be carefully assessed on a case by case basis.

3.3. Artificial corner reflectors

The lack of PSs or a low PS density over a given area can be mitigated by deploying artificial Corner Reflectors (CRs). These devices, installed in situ, provide a strong response in the SAR images resulting in good interferometric phases to derive the deformation estimates (Sarabandi and Chiu, 1996; Doerry, 2008). By using CRs, it is possible to strategically locate the deformation measurement points, although this approach requires access to the area of interest to install the CRs and, thus, deviates from pure satellite-based remote sensing. The CRs can be installed permanently in situ. In this case their integrity has to be guaranteed over the entire monitoring period. Alternatively, the CRs can be mounted and dismounted at each image acquisition. Some technical aspects of DInSAR monitoring using CRs are described in Xia et al. (2002) and Crosetto et al. (2013). CRs have been used in different studies to assess the performance of DInSAR and PSI (Ferretti et al., 2007; Marinkovic et al., 2007; Quin and Loreaux, 2013). They have also been employed in several PSI applications, e.g. see van Leijen and Hanssen (2007), Wegmüller et al. (2010), Daqing et al. (2011), Teatini et al. (2012) and Yu et al. (2013).

3.4. Maximum deformation rates and linear deformation model

PSI suffers severe limitations in the capability to measure "fast" deformation phenomena due to the ambiguous nature of its observations, i.e. the wrapped interferometric phases. Considering the simplified Eq. (7), and computing the phase difference between two PSs, i and j:

$$\Delta\Delta\varphi^{i,j}_{D\text{-}Int} = \Delta\varphi^{i,j}_{Displ} \tag{9}$$

The limitation due to the ambiguous nature of the observation is severe. In fact, when the differential DInSAR deformation phase $\Delta\varphi^{i,j}_{Displ}$ between two subsequent acquisitions is bigger than π, the

Fig. 3. Comparison of the Persistent Scatterer (PS) density achievable using C-band (Envisat) and X-band (TerraSAR-X) PSI.

actual deformation cannot be retrieved unambiguously. The limit of π on the differential phases corresponds to a maximum differential deformation of $\lambda/4$ over the revisit interval. Considering their wavelength and revisiting time, the maximum differential deformation rate measurable is 14.7, 25.7, 42.6 and 46.8 cm/yr for Envisat, TerraSAR-X, Sentinel-1 and ALOS, respectively. These are theoretical values; the actual capability to estimate the deformation rates depends on the noise level of the data and the specific phase unwrapping technique used to resolve phase ambiguities (van Leijen, 2014). It is important to note that the abovementioned condition concerns differential phases, i.e. phases computed over pairs of PSs. The actual capability to measure deformation over a given PS depends on the spatial pattern of the specific deformation phenomenon at hand (the smoother this pattern, the better) and the available PS density over this phenomenon (the higher the density, the better). For all phenomena whose deformation largely exceeds the abovementioned limit, it is possible to complement the PSI measurements using SAR amplitude-based techniques, e.g. see Casu et al. (2011). The idea is to exploit the SAR amplitude information of at least two SAR images, acquired at different times, by estimating 2D displacements (pixel offsets), across-track (range) and along-track (azimuth), of given targets. This requires the use of image matching techniques. It is worth noting that this approach yields 2D deformation measurements, which are not affected by the ambiguous nature of the interferometric approaches. Its main limitation is the low sensitivity to deformation, which is a fraction of the SAR pixel footprint (e.g. 1/10th or 1/20th of the pixel, see Fialko et al. (2001) and Strozzi et al. (2002)) and depends on the local SAR amplitude contrast. Many PSI approaches use a linear deformation model in their deformation estimation procedures, see Table 1. For instance, the PSI deformation products generated in the Terrafirma project (http://www.terrafirma.eu.com) were based on this model. This assumption, which is required to unwrap the interferometric phases, can have a negative impact on the deformation estimates of all phenomena characterized by non-linear deformation behaviour, where the assumption is not valid. The PSI products based on the linear assumption typically lack PSs in all areas where the deformation shows significantly non-linear motion, because there is a misfit between the linear model and the observed (non-linear) deformation. Note that this can be a critical aspect because it affects the areas where the interest to measure deformation is highest,

Please cite this article in press as: Crosetto, M., et al. Persistent Scatterer Interferometry: A review. ISPRS J. Photogram. Remote Sensing (2015), http://dx.doi.org/10.1016/j.isprsjprs.2015.10.011

representing a limitation to the applicability of PSI. Several PSI approaches do not use a linear deformation model, see Table 1, assuming a spatial smoothness of the observed deformation phenomena. However, it is worth to underline that these methods suffer the limitation related to the ambiguous nature of the phases, which is described above.

3.5. Deformation time series

The deformation time series represent the most advanced PSI product. They provide the deformation history over the observed period, which is fundamental for many applications, e.g. studying the kinematics of a given phenomenon (quiescence, activation, acceleration, etc.), correlation with driving factors, etc. In order to properly use, interpret and exploit the deformation time series it is important to consider that they are a zero-redundancy product. In fact, they contain one deformation estimate per each SAR acquisition, i.e. per each observation. For this reason, they are particularly sensitive to the phase noise. This aspect was highlighted in the Terrafirma Validation project analysing C-band ERS and Envisat data (Crosetto et al., 2008b). X-band time series show a remarkable quality improvement over C-band time series, e.g. see (Crosetto et al., 2010). It is important to consider that, if used, the linear deformation model can considerably dominate the time series patterns and this issue needs to be carefully considered during data interpretation. Note that some PSI approaches do not use any linear deformation model, see Table 1.

3.6. Line-of-sight deformation measurements

PSI deformation measurements refer to the LOS of the SAR sensor, i.e. the line that connects the sensor and the target at hand. Given a generic 3D deformation, PSI provides the estimate of one component of this deformation, which is obtained by projecting the 3D deformation into the LOS direction. The 1D nature of the measurements represents an important limitation of DInSAR and PSI. Several works have been devoted to resolve 2D and 3D displacements from DInSAR measurements. 2D measurements (along-tack and in the LOS) can be derived using the multi-aperture InSAR approach (Bechor and Zebker, 2006) or offset-tracking (Casu et al., 2011). The vertical and east-to-west horizontal components of deformation can be retrieved when ascending and descending SAR data are available, e.g. see Ferretti et al. (2007). This requires an independent processing of the ascending and descending datasets. Different methods have been proposed to derive 3D deformation measurements from DInSAR, see Hu et al. (2014) for a review, by combining satellite passes with different incidence angles, by integrating DInSAR and GPS data or by making an assumption on the direction of the 3D deformation. The latter one is the most widely used, e.g. see Joughin et al. (1998), Colesanti and Wasowski (2006), Samieie-Esfahany et al. (2009) and Cascini et al. (2010).

3.7. Deformation tilts/trends

The PSI deformation velocity maps can sometimes be affected by tilts, which can be caused by uncompensated orbital errors or uncompensated low frequency atmospheric effects, e.g. see Bateson et al. (2010). Note that these tilts have a corresponding effect in the deformation time series. A tilt in a given deformation velocity map could be due to uncompensated processing errors or to a real geophysical signal. One of the following two situations could happen: (i) a tilt in a given velocity map can be interpreted as geophysical signal, while in fact it is simply a result of residual processing errors, which can have a negative impact in the results of the geophysical analysis at hand; (ii) a tilt-free velocity map can be interpreted by a geophysicist as no signal, e.g. quiescence of a given phenomenon, while in fact the site may have undergone significant geophysical low-frequency deformations that have been removed (together with the other residual effects) during the PSI processing. Any PSI application focused on low spatial-frequency deformation signals should consider this limitation of the PSI technique. However, this limitation can be overcome by using multiple overlapping tracks or by fusing the PSI with external data from GNSS, levelling, gravimetry, etc., e.g. see Chen et al. (2010), Hung et al. (2011), Caro Cuenca et al. (2011), Hanssen et al. (2012) and Adam et al. (2013).

3.8. Thermal expansion component of PSI observations

Due to the high sensitivity to subtle deformations, the interferometric phases might contain a non-negligible component related to thermal expansion, i.e. to the displacements that are caused by temperature differences in the imaged area between SAR acquisitions. This issue has been reported in some studies with C-band PSI, e.g. Ferretti et al. (2005), Perissin and Rocca (2006) and Crosetto et al. (2008a), referring mainly to single PSs. With X-band PSI, the thermal expansion is evident over large sets of PSs, which enables the analysis and interpretation of the thermal expansion signal of single objects such as buildings and bridges. Two strategies can be used with respect to the thermal expansion. The simplest one is to perform the standard PSI analysis implicitly including the thermal expansion in the total observed displacement, e.g. see Crosetto et al. (2008a). However, especially in X-band, this has an important disadvantage because if the thermal expansion is not explicitly modelled, the PSI deformation products can be affected by strong distortions, which can be particularly severe if limited PSI datasets in relatively short periods are analysed (Crosetto et al., 2015). The second strategy is to explicitly model and estimate the thermal expansion, see Gernhardt et al. (2010), Monserrat et al. (2011), Fornaro et al. (2013) and Zhang et al. (2014). Monserrat et al. (2011) and Crosetto et al. (2015) describe how to use the maps of the estimated thermal expansion parameter, called thermal maps. They can be used to derive the thermal expansion coefficient of the observed objects and information on the static structure of the same objects.

4. PSI validation

The validation of PSI has received a lot of attention in the last fifteen years. Its results have provided valuable inputs for the research on PSI and development activities, and have proved to be key for the acceptability of this new technique at scientific, technical and commercial level. Most of the PSI validation activities were based on the comparison of deformation velocities and time series with independent estimations of the same quantities acquired by sources of better quality, e.g. levelling or GPS measurements. Two major validation exercises were organized by the European Space Agency: PSIC4 (earth.esa.int/psic4; Raucoules et al., 2009), and the Terrafirma Validation Project (www.terrafirma.eu.com/Terrafirma_validation.htm; Crosetto et al., 2009). Interesting results were obtained in the Terrafirma Validation Project by inter-comparing the PSI results from different teams, which were derived using the same stacks of ERS and Envisat data. The intercomparison was based on vast sets of common PSs, i.e. PSs where at least two teams provided their PSI estimates (velocity, time series and RSE). From the standard deviation (σ) of the velocity differences, assuming the same precision for the compared teams and uncorrelated errors between teams, the estimated σ of the deformation velocity was:

$$\sigma_{Velo} = 0.4 - 0.5 \text{ mm/yr}. \quad (10)$$

Please cite this article in press as: Crosetto, M., et al. Persistent Scatterer Interferometry: A review. ISPRS J. Photogram. Remote Sensing (2015), http://dx.doi.org/10.1016/j.isprsjprs.2015.10.011

Using a similar procedure for the time series, the estimated σ of the deformation time series was:

$$\sigma_{TSeries} = 1.1 - 4 \text{ mm}. \quad (11)$$

It is worth noting that such numbers describe the dispersion of the results of different PSI chains based on exactly the same input data stacks. This dispersion reflects the fact that PSI involves a complex estimation process: even starting with exactly the same data, different processes generate different errors and hence different results. The above values provide information on the global behaviour of PSI velocities and time series for the ERS and Envisat data. It is however important to underline that they are only representative of areas with characteristics similar to those of the Terrafirma Validation Project test sites, i.e. urban areas with zero or moderate deformation velocities.

Some preliminary considerations are made prior to briefly reviewing the most relevant PSI validation works. Firstly, in order to properly assess the performance of PSI, it is worth considering that PSI is a rather complex process, whose results depend on multiple factors, e.g. the SAR sensor, the number of available SAR images, the PS density and quality, the characteristics of the deformation at hand (spatial extent, type of temporal deformation, deformation rates, etc.), the distance from the reference point, the quality of the reference point, etc. The best PSI performances are obtained under ideal conditions, i.e. large data stacks, high PS density, zero to slow deformation, etc. This is for instance the case of the inter-comparison values mentioned above and the experiment using two dihedral reflectors described in Ferretti et al. (2007), where sub-millimeter accuracy was obtained in the DInSAR time series: these results were achieved under optimal conditions (high quality PSs, minimum atmospheric effects, etc.). However, these performances cannot be generalized to every possible PSI scenario: in fact, the performances tend to worsen when the conditions deviate from the optimal ones. Secondly, it is worth underlining the complexity of the PSI outputs, especially the deformation time series: it is often difficult to obtain appropriate ground truth for validation purposes. Thirdly, many validation results refer to single PSs while several applications concern low-spatial frequency phenomena, where PSI can usually offer a dense PS sampling. The PS spatial data redundancy is a clear advantage of PSI with respect to other point wise measurement techniques.

Some of the most relevant PSI validation works are considered here. A validation based on the intermediate products of different PSI chains, which was carried out in the Terrafirma Validation Project, is described in Adam et al. (2009). Two works describe experiments based on CRs performed under optimal PSI conditions: Marinkovic et al. (2007) report a σ of the double differences along the vertical of 1.6 mm and 2.6 mm for Envisat and ERS data, respectively, using levelling data, and Quin and Loreaux (2013) report a σ of the TerraSAR-X LOS time series of 0.48 mm using micrometers. Several works describe validation results of deformation velocity and time series, mainly based on levelling and GPS data. Musson et al. (2004) show the comparison between ERS deformation velocities with values derived by GPS, obtaining differences below 0.5 mm/yr. Hooper et al. (2004) describe validation results in a volcanic application, where a good agreement in the vertical motion was obtained between PSI and topographic data. Colesanti et al. (2005) describe a validation carried out in a mining area. This work shows the limitation of PSI with fast and decimetric deformation occurring during collapse events (i.e. far from the ideal PSI condition mentioned above). Casu et al. (2006) describe the validation of the SBAS technique with ERS data, obtaining a σ of the velocity differences of 1 mm/yr and a σ of 5 mm for the deformation time series. Heleno et al. (2011) describe the inter-comparison of the results from two independent PSI chains, and their validation using levelling and GPS data. Finally, Liu et al. (2014a) describe the validation of TerraSAR-X PSI results, reporting a σ of the deformation time series of about 3 mm. A special mention is deserved to the RTE, which is a key parameter for PS geocoding. In the Terrafirma Validation Project, using the same inter-comparison approach employed for the deformation velocity, the σ of RTE was estimated to range between 0.9 and 2.0 m. Considering the acquisition geometry of ERS and Envisat, this results in a geocoding σ that ranges between 2.1 and 4.7 m. These values only reflect the direct effect of the RTE dispersion, which roughly affects the east to west direction (the direction perpendicular to the SAR track). Two works focused on the RTE are Perissin and Rocca (2006) and Perissin (2008).

Table 2
Classification of the most important PSI applications, with references for each application.

Main classes	Sub-classes	Data source and references
Urban, peri-urban, built	Urban and peri-urban areas	ERS-Lanari et al. (2004b); ERS-Vallone et al. (2008); ERS/ENV-Herrera et al. (2009a); TSX-Gernhardt et al. (2010)
	Infrastructures	TSX-Lan et al. (2012); ERS-Sousa and Bastos (2013); TSX-Crosetto et al. (2015); ERS/ENV/TSX-Wasowski et al. (2015)
	Buildings	TSX-Gernhardt and Bamler (2012); ERS/ENV-Karila et al. (2013); TSX-Gernhardt et al. (2015)
	Dam monitoring	ERS/ENV-Tomás et al. (2013); ENV-Di Martire et al. (2014)
	Cultural Heritage	ERS/ENV-Tapete and Cigna (2012); ERS/ENV/RS1-Cigna et al. (2013a); ERS/ENV/RS1-Pratesi et al. (2015)
	Construction works	ENV-Zhao et al. (2009); TSX-Strozzi et al. (2009); TSX-Liu et al. (2014b)
	Reclaimed land	ENV-Kim et al. (2010); ENV-Jiang et al. (2011)
Subsidence/uplift	Mining	ERS-Colesanti et al. (2005); ERS/ENV-Herrera et al. (2007); ENV-Biescas et al. (2007); ERS-Raucoules et al. (2009); TSX-Wegmüller et al. (2010)
	Groundwater abstraction/recharge	ERS-Schmidt and Bürgmann (2003); ERS-Ferretti et al. (2004); ERS-Zerbini et al. (2007); ERS/ENV-Bell et al. (2008)
	Reservoir	ENV-Vasco et al. (2008); ENV-Vasco et al. (2010); RS1-Teatini et al. (2011)
	Flood risk	RS1-Dixon et al. (2006); ERS/ENV-Teatini et al. (2012)
Landslides	Inventory	ERS-Cascini et al. (2010); TSX-Notti et al. (2010); ERS/ENV-Righini et al. (2012)
	Monitoring	ERS-Farina et al. (2006); ERS/ENV-Herrera et al. (2009b); ERS/ENV-Tofani et al. (2013)
	Analysis and modelling	ENV/TSX-Herrera et al. (2011); CSK-Bovenga et al. (2012); ERS/ENV-Rosi et al. (2013); ERS/ENV/RS1-Cigna et al. (2013b)
Geophysics	Tectonics	ERS-Bürgmann et al. (2006); ERS-Lanari et al. (2007b); ERS-Funning et al. (2007); ERS-Motagh et al. (2007); CSK-Reale et al. (2011);
	Vulcanology	ERS- Hooper et al. (2004); ERS-Lundgren et al. (2004); ERS-Hooper et al. (2009)

Please cite this article in press as: Crosetto, M., et al. Persistent Scatterer Interferometry: A review. ISPRS J. Photogram. Remote Sensing (2015), http://dx.doi.org/10.1016/j.isprsjprs.2015.10.011

5. Review of main PSI applications

The potential of the PSI technique has been recognized since it was first proposed (Ferretti et al., 2001). In the last fifteen years, a wide range of PSI applications has been developed. A classification of the most important PSI applications is provided in Table 2, which refers to four main and partially overlapping classes: (i) urban, peri-urban and built; (ii) subsidence and uplift; (iii) landslides; and (iv) geophysics. Each class is divided in sub-classes, providing a few references for each application.

PSI applications exploit the main advantages of the technique. Firstly, PSI offers wide-area coverage associated with a relatively high spatial measurement density. This allows studying wide areas (e.g. 100 by 100 km with single frames of StripMap ERS and Envisat, 250 by 250 km with single frames of the Interferometric Wide Swath of Sentinel-1), thus getting a global outlook of the deformation phenomena in the imaged areas. At the same time, PSI keeps the capability to measure individual infrastructures, buildings, small-area deformation phenomena, etc. This capability is particularly evident using very high-resolution X-band data. In fact, the availability of this type of data since 2007 has remarkably increased the application potential of PSI. Secondly, PSI has a high sensitivity to small deformations, which is fundamental for the majority of the PSI applications. Thirdly, an unmatched capability is given by the ability to measure past deformation phenomena by using the SAR image historical archives. This unique aspect means that it is possible to study deformation phenomena that occurred in the past and for which no other survey data are available. However, image availability varies very much from one mission to another, and is strongly uneven around the globe. Fourthly, PSI enables the possibility of obtaining a potential reduction in the amount of ground-based observations, achieving simplified logistics operations and reducing personnel time and costs. Finally, it is worth mentioning that Sentinel-1 data are freely available, which represents an additional advantage in order to facilitate the development of new PSI applications. The major challenge for the PSI community is to develop new tools to process and analyse the huge amount of data acquired by this sensor.

6. Conclusions and outlook

PSI is a remote sensing technique able to measure millimetric displacements of the Earth's surface from space. This amazing fact has been widely demonstrated by several PSI research teams and commercial companies and is documented by hundreds of high-quality scientific papers and publications. Since the introduction of the first PSI technique (Ferretti et al., 2000, 2001), a lot of research and development activities have been carried out. About 20 different PSI approaches are described in this paper, but the number is surely larger and it will increase in the future. The technical improvements achieved so far concern all main PSI components: (i) advances in the pixel selection to increase the density and quality of the PSI measurements, e.g. distributed scatterers, partially coherent targets, etc.; (ii) improvement in the 2D and 3D phase unwrapping algorithms; (iii) the use of more flexible and accurate deformation models; (iv) the improvement in the algorithms to estimate the atmospheric phase component; (v) the ability to generate wide-area deformation products; etc. The potential of the PSI technique can be highlighted from two points of view. The first one is given by the PSI validation results, which have been reviewed in this work. These results are useful to get an assessment of the high sensitivity, precision and accuracy of the PSI products. The reader is however warned to consider that the PSI is a rather complex process and that its performance depends on multiple factors (SAR sensor, number of SAR images, PS density, characteristics of the deformation at hand, etc.). The second point of view is given by the wide spectrum of PSI applications that are described in the literature and are briefly reviewed in this paper. An additional and important factor for the success of PSI is the current availability of several active SAR missions and the plans of several space agencies to guarantee the continuity of these missions in the future.

The main open PSI problems and future research lines are:

- Despite the tremendous research and development effort of the last fifteen years, there is surely room for improvement. In fact, the different PSI approaches might still gain flexibility and reliability. One of the most important components to be improved is phase unwrapping: more flexible and robust methods able to warn the user when the phase ambiguity estimation, and hence the deformation estimation, is failing or likely to fail, are needed.
- The different PSI approaches often lack a full characterization of the quality of their processing steps. There is, in general, a need to fully characterize the uncertainty associated with the main components of the PSI data processing and of the different PSI products. An important contribution in this direction is given by the geodetic approach described in van Leijen (2014).
- The different PSI approaches have different degrees of maturity and performances. In order to correctly inform the potential users and to increase the acceptability of the technique, it would be useful to promote new exercises of inter-comparisons of the results obtained from different PSI approaches, such as the one carried out in the Terrafirma Validation Project.
- The data acquisition capability of the SAR sensors largely exceeds the throughput of all the available PSI systems. There is a need to increase the processing capability of current PSI algorithms. This involves augmenting their degree of automation, speeding up the quality control of the different PSI processing steps. The objective is to achieve a massive data processing capability to systematically monitor very wide areas.
- In parallel to the previous point, there is the need to improve the capability to exploit the PSI results. In fact, the added value of PSI largely relies on the interpretation and exploitation of its deformation measurements. Even though this is not always the case, the PSI exploitation is often in the hands of non PSI experts that may ignore that several features of the PSI products are not common to other deformation measurement techniques, e.g. the opportunistic PSI sampling, the phase unwrapping errors, the residual trends in the velocity maps, etc. In order to increase the PSI exploitation capability, there is a need to properly document and communicate the characteristics and peculiarities of PSI products. Additionally, it is desirable to increase the collaboration between PSI experts and people in charge of the interpretation and exploitation of the PSI results. These two activities are required to increase the acceptability of the PSI technique in different technical sectors, e.g. geomatics, and in particular the deformation monitoring community, civil engineering, geotechnics, engineering geology, geology, natural risk management, etc.

Acknowledgement

This work has been partially funded by the Spanish Ministry of Economy and Competitiveness through the project MIDES (Ref: CGL2013-43000-P).

References

Adam, N., Parizzi, A., Eineder, M., Crosetto, M., 2009. Practical persistent scatterer processing validation in the course of the Terrafirma project. J. Appl. Geophys. 69 (1), 59–65.

Adam, N., Rodriguez Gonzalez, F., Parizzi, A., Liebhart, W., 2011. Wide area persistent scatterer interferometry. In: Proceedings of IGARSS 2011. Vancouver, pp. 1481–1484.

Adam, N., Rodriguez Gonzalez, F., Parizzi, A., Brcic, R., 2013. Wide area persistent scatterer interferometry: current developments, algorithms and examples. In: Proceedings of IGARSS 2013. Melbourne, pp. 1857–1860.

Agram, P.S., Jolivet, R., Riel, B., Lin, Y.N., Simons, M., Hetland, E., Doin, M.P., Lasserre, C., 2013. New radar interferometric time series analysis toolbox released. Eos, Trans. Am. Geophys. Union 94 (7), 69–70.

Alshawaf, F., Hinz, S., Mayer, M., Meyer, F., 2015. Constructing accurate maps of atmospheric water vapor by combining interferometric synthetic aperture radar and GNSS observations. J. Geophys. Res.: Atmos. 120 (4), 1391–1403.

Amelung, F., Galloway, D.L., Bell, J.W., Zebker, H.A., Laczniak, R.J., 1999. Sensing the ups and downs of Las Vegas: InSAR reveals structural control of land subsidence and aquifer-system deformation. Geology 27 (6), 483–486.

Antonielli, B., Monserrat, O., Bonini, M., Righini, G., Sani, F., Luzi, G., Feyzullayev, A. A., Aliyev, C.S., 2014. Pre-eruptive ground deformation of Azerbaijan mud volcanoes detected through satellite radar interferometry (DInSAR). Tectonophysics 637, 163–177.

Auer, S., Hinz, S., Bamler, R., 2010. Ray-tracing simulation techniques for understanding high-resolution SAR images. IEEE TGRS 48 (3), 1445–1456.

Auer, S., Gernhardt, S., Bamler, R., 2011. Ghost persistent scatterers related to multiple signal reflections. IEEE Geosci. Remote Sens. Lett. 8 (5), 919–923.

Bamler, R., Hartl, P., 1998. Synthetic aperture radar interferometry. Inverse Probl. 14, R1–R54.

Basilico, M., Ferretti, A., Novali, F., Prati, C., Rocca, F., 2004. Advances in permanent scatterers analysis: semi and temporary PS. In: Proc. Eur. Conf. Synthetic Aperture Radar, pp. 25–27.

Bateson, L., Novali, F., Cooksley, G., 2010. Terrafirma user guide: a guide to the use and understanding of Persistent Scatterer Interferometry in the detection and monitoring of terrain-motion. Terrafirma project, ESRIN/Contract no. 19366/05/I-E, available on-line at <www.terrafirma.eu.com/users.htm>.

Bechor, N.B., Zebker, H.A., 2006. Measuring two-dimensional movements using a single InSAR pair. Geophys. Res. Lett. 33 (16).

Bell, J.W., Amelung, F., Ferretti, A., Bianchi, M., Novali, F., 2008. Permanent scatterer InSAR reveals seasonal and long-term aquifer-system response to groundwater pumping and artificial recharge. Water Resour. Res. 44 (2).

Berardino, P., Fornaro, G., Lanari, R., Sansosti, E., 2002. A new algorithm for surface deformation monitoring based on small baseline differential SAR interferograms. IEEE TGRS 40 (11), 2375–2383.

Biescas, E., Crosetto, M., Agudo, M., Monserrat, O., Crippa, B., 2007. Two radar interferometric approaches to monitor slow and fast land deformation. J. Surv. Eng. 133 (2), 66–71.

Bovenga, F., Wasowski, J., Nitti, D.O., Nutricato, R., Chiaradia, M.T., 2012. Using COSMO/SkyMed X-band and ENVISAT C-band SAR interferometry for landslides analysis. Remote Sens. Environ. 119, 272–285.

Bürgmann, R., Hilley, G., Ferretti, A., Novali, F., 2006. Resolving vertical tectonics in the San Francisco Bay Area from permanent scatterer InSAR and GPS analysis. Geology 34 (3), 221–224.

Carnec, C., Massonnet, D., King, C., 1996. Two examples of the use of SAR interferometry on displacement fields of small spatial extent. Geophys. Res. Lett. 23 (24), 3579–3582.

Caro Cuenca, M., Hanssen, R., Hooper, A., Arıkan, M., 2011. Surface deformation of the whole Netherlands after PSI analysis. In: Proceedings of FRINGE 2011, Frascati, Italy.

Cascini, L., Fornaro, G., Peduto, D., 2010. Advanced low-and full-resolution DInSAR map generation for slow-moving landslide analysis at different scales. Eng. Geol. 112 (1), 29–42.

Casu, F., Manzo, M., Lanari, R., 2006. A quantitative assessment of the SBAS algorithm performance for surface deformation retrieval from DInSAR data. Remote Sens. Environ. 102 (3), 195–210.

Casu, F., Manconi, A., Pepe, A., Lanari, R., 2011. Deformation time-series generation in areas characterized by large displacement dynamics: the SAR amplitude pixel-offset SBAS technique. IEEE TGRS 49 (7), 2752–2763.

Catalao, J., Nico, G., Hanssen, R., Catita, C., 2011. Merging GPS and atmospherically corrected InSAR data to map 3-D terrain displacement velocity. IEEE TGRS 49 (6), 2354–2360.

Chen, Q., Liu, G., Ding, X., Hu, J.C., Yuan, L., Zhong, P., Omura, M., 2010. Tight integration of GPS observations and persistent scatterer InSAR for detecting vertical ground motion in Hong Kong. Int. J. Appl. Earth Obs. Geoinform. 12 (6), 477–486.

Cigna, F., Liguori, V., Del Ventisette, C., Casagli, N., 2013a. Landslide impacts on Agrigento's Cathedral imaged with radar interferometry. In: Landslide Science and Practice. Springer, Berlin, Heidelberg, pp. 475–481.

Cigna, F., Bianchini, S., Casagli, N., 2013b. How to assess landslide activity and intensity with Persistent Scatterer Interferometry (PSI): the PSI-based matrix approach. Landslides 10 (3), 267–283.

Colesanti, C., Ferretti, A., Novali, F., Prati, C., Rocca, F., 2003. SAR monitoring of progressive and seasonal ground deformation using the Permanent Scatterers Technique. IEEE TGRS 41 (7), 1685–1701.

Colesanti, C., Mouelic, S.L., Bennani, M., Raucoules, D., Carnec, C., Ferretti, A., 2005. Detection of mining related ground instabilities using the Permanent Scatterers technique—a case study in the east of France. Int. J. Remote Sens. 26 (1), 201–207.

Colesanti, C., Wasowski, J., 2006. Investigating landslides with space-borne Synthetic Aperture Radar (SAR) interferometry. Eng. Geol. 88 (3), 173–199.

Costantini, M., Malvarosa, F., Minati, F., Pietranera, L., Milillo, G., 2002. A three-dimensional phase unwrapping algorithm for processing of multitemporal SAR interferometric measurements. In: Proceedings of IGARSS 2002, Toronto.

Costantini, M., Falco, S., Malvarosa, F., Minati, F., 2008. A new method for identification and analysis of persistent scatterers in series of SAR images. In: Proceedings of IGARSS 2008, Boston.

Costantini, M., Malvarosa, F., Minati, F., Vecchioli, F., 2012. Multi-scale and block decomposition methods for finite difference integration and phase unwrapping of very large datasets in high resolution SAR interferometry. In: Proceedings of IGARSS 2012, Munich, pp. 5574–5577.

Costantini, M., Falco, S., Malvarosa, F., Minati, F., Trillo, F., Vecchioli, F., 2014. Persistent scatterer pair interferometry: approach and application to COSMO-SkyMed SAR data. J. Select. Top. Appl. Earth Obs. Remote Sens. 7 (7), 2869–2879.

Crosetto, M., Crippa, B., Biescas, E., 2005. Early detection and in-depth analysis of deformation phenomena by radar interferometry. Eng. Geol. 79, 81–91.

Crosetto, M., Biescas, E., Duro, J., Closa, J., Arnaud, A., 2008a. Generation of advanced ERS and Envisat interferometric SAR products using the stable point network technique. Photogram. Eng. Remote Sens. 74 (4), 443–450.

Crosetto, M., Monserrat, O., Adam, N., Parizzi, A., Bremmer, C., Dortland, S., Hanssen, R.F., van Leijen, F., 2008b. Final report of the Validation of existing processing chains in Terrafirma stage 2. Terrafirma project, ESRIN/Contract no. 19366/05/I-E, available on-line at <www.terrafirma.eu.com/Terrafirma_validation.htm>.

Crosetto, M., Monserrat, O., Bremmer, C., Hanssen, R., Capes, R., Marsh, S., 2009. Ground motion monitoring using SAR interferometry: quality assessment. Eur. Geol. 26, 12–15.

Crosetto, M., Monserrat, O., Iglesias, R., Crippa, B., 2010. Persistent Scatterer Interferometry: potential, limits and initial C- and X-band comparison. Photogram. Eng. Remote Sens. 76 (9), 1061–1069.

Crosetto, M., Gili, J.A., Monserrat, O., Cuevas-González, M., Corominas, J., Serral, D., 2013. Interferometric SAR monitoring of the Vallcebre landslide (Spain) using corner reflectors. Nat. Hazards Earth Syst. Sci. 13 (4), 923–933.

Crosetto, M., Monserrat, O., Cuevas-González, M., Devanthéry, N., Luzi, G., Crippa, B., 2015. Measuring thermal expansion using X-band persistent scatterer interferometry. ISPRS J. 100, 84–91.

Dalla Via, G., Crosetto, M., Crippa, B., 2012. Resolving vertical and east-west horizontal motion from differential interferometric synthetic aperture radar: the L'Aquila earthquake. J. Geophys. Res.: Solid Earth (1978–2012) 117 (B2).

Daqing, G., Yan, W., Ling, Z., Xuedong, Z., Dapeng, Y., Man, L., 2011. Integrating corner reflectors and PSInSAR technique to monitor regional land subsidence. In: Proceedings of IGARSS 2011, Vancouver.

Devanthéry, N., Crosetto, M., Monserrat, O., Cuevas-González, M., Crippa, B., 2014. An approach to persistent scatterer interferometry. Remote Sens. 6 (7), 6662–6679.

De Zan, F., Monti Guarnieri, A., 2006. TOPSAR: terrain observation by progressive scans. IEEE TGRS 44 (9), 2352–2360.

Dheenathayalan, P., Caro Cuenca, M., Hanssen, R., 2011. Different approaches for PSI target characterization for monitoring urban infrastructure. In: Proceedings of FRINGE 2011, Frascati (Italy).

Di Martire, D., Iglesias, R., Monells, D., Centolanza, G., Sica, S., Ramondini, M., Pagano, L., Mallorquí, J.J., Calcaterra, D., 2014. Comparison between differential SAR interferometry and ground measurements data in the displacement monitoring of the earth-dam of Conza della Campania (Italy). Remote Sens. Environ. 148, 58–69.

Dixon, T.H., Amelung, F., Ferretti, A., Novali, F., Rocca, F., Dokka, R., Sella, G., Kim, S. W., Wdowinski, S., Whitman, D., 2006. Space geodesy: subsidence and flooding in New Orleans. Nature 441 (7093), 587–588.

Doerry, A.W., 2008. Reflectors for SAR performance testing. Sandia Report SAND2008-0396, Unlimited Release.

Duro, J., Inglada, J., Closa, J., Adam, N., Arnaud, A., 2003. High resolution differential interferometry using time series of ERS and ENVISAT SAR data. In: FRINGE 2003 Workshop, vol. 550, p. 72.

Eineder, M., Adam, N., Bamler, R., Yague-Martinez, N., Breit, H., 2009. Spaceborne spotlight SAR interferometry with TerraSAR-X. IEEE TGRS 47 (5), 1524–1535.

Farina, P., Colombo, D., Fumagalli, A., Marks, F., Moretti, S., 2006. Permanent scatterers for landslide investigations: outcomes from the ESA-SLAM project. Eng. Geol. 88 (3), 200–217.

Ferretti, A., Prati, C., Rocca, F., 2000. Nonlinear subsidence rate estimation using permanent scatterers in differential SAR interferometry. IEEE TGRS 38 (5), 2202–2212.

Ferretti, A., Prati, C., Rocca, F., 2001. Permanent scatterers in SAR interferometry. IEEE TGRS 39 (1), 8–20.

Ferretti, A., Novali, F., Bürgmann, R., Hilley, G., Prati, C., 2004. InSAR permanent scatterer analysis reveals ups and downs in San Francisco Bay area. Eos, Trans. Am. Geophys. Union 85 (34), 317–324.

Ferretti, A., Perissin, D., Prati, C., Rocca, F., 2005. On the physical nature of SAR permanent scatterers. In: Proceedings of URSI Commission F Symposium on Microwave Remote Sensing of the Earth, Oceans, Ice and Atmosphere, Ispra, Italy.

Ferretti, A., Savio, G., Barzaghi, R., Borghi, A., Musazzi, S., Novali, F., Prati, C., Rocca, F., 2007. Submillimeter accuracy of InSAR time series: experimental validation. IEEE TGRS 45 (5), 1142–1153.

Ferretti, A., Fumagalli, A., Novali, F., Prati, C., Rocca, F., Rucci, A., 2011. A new algorithm for processing interferometric data-stacks: SqueeSAR. IEEE TGRS 49 (9), 3460–3470.

Please cite this article in press as: Crosetto, M., et al. Persistent Scatterer Interferometry: A review. ISPRS J. Photogram. Remote Sensing (2015), http://dx.doi.org/10.1016/j.isprsjprs.2015.10.011

Fialko, Y., Simons, M., Agnew, D., 2001. The complete (3-D) surface displacement field in the epicentral area of the 1999 M_W7. 1 Hector Mine Earthquake, California, from space geodetic observations. Geophys. Res. Lett. 28 (16), 3063–3066.

Fornaro, G., Pauciullo, A., Reale, D., 2011. A null-space method for the phase unwrapping of multitemporal SAR interferometric stacks. IEEE TGRS 49 (6), 2323–2334.

Fornaro, G., Reale, D., Verde, S., 2013. Bridge thermal dilation monitoring with millimeter sensitivity via multidimensional SAR imaging. IEEE Geosci. Remote Sens. Lett. 10, 677–681.

Fornaro, G., D'Agostino, N., Giuliani, R., Noviello, C., Reale, D., Verde, S., 2014. Assimilation of GPS-derived atmospheric propagation delay in DInSAR data processing. J. Select. Top. Appl. Earth Obs. Remote Sens. 8 (2), 784–799.

Funning, G.J., Bürgmann, R., Ferretti, A., Novali, F., Fumagalli, A., 2007. Creep on the Rodgers Creek fault, northern San Francisco Bay area from a 10 year PS-InSAR dataset. Geophys. Res. Lett. 34 (19).

Gabriel, A.K., Goldstein, R.M., Zebker, H.A., 1989. Mapping small elevation changes over large areas: differential radar interferometry. J. Geophys. Res. 94 (B7), 9183–9191.

Galloway, D.L., Hudnut, K.W., Ingebritsen, S.E., Phillips, S.P., Peltzer, G., Rogez, F., Rosen, P.A., 1998. Detection of aquifer system compaction and land subsidence using interferometric synthetic aperture radar, Antelope Valley, Mojave Desert, California. Water Resour. Res. 34 (10), 2573–2585.

García-Davalillo, J.C., Herrera, G., Notti, D., Strozzi, T., Álvarez-Fernández, I., 2014. DInSAR analysis of ALOS PALSAR images for the assessment of very slow landslides: the Tena Valley case study. Landslides 11 (2), 225–246.

Gernhardt, S., Adam, N., Eineder, M., Bamler, R., 2010. Potential of very high resolution SAR for persistent scatterer interferometry in urban areas. Ann. GIS 16 (2), 103–111.

Gernhardt, S., Bamler, R., 2012. Deformation monitoring of single buildings using meter-resolution SAR data in PSI. ISPRS J. 73, 68–79.

Gernhardt, S., Auer, S., Eder, K., 2015. Persistent scatterers at building facades – evaluation of appearance and localization accuracy. ISPRS J. 100, 92–105.

Ghiglia, D.C., Pritt, M.D., 1998. Two-dimensional Phase Unwrapping: Theory, Algorithms, and Software. Wiley, New York.

Goel, K., Adam, N., 2014. A distributed scatterer interferometry approach for precision monitoring of known surface deformation phenomena. IEEE TGRS 52 (9), 5454–5468.

Goldstein, R.M., Engelhardt, H., Kamb, B., Frolich, R.M., 1993. Satellite radar interferometry for monitoring ice sheet motion: application to an Antarctic ice stream. Science 262 (5139), 1525–1530.

Hanssen, R., 2001. Radar Interferometry. Kluwer Academic Publishers, Dordrecht, The Netherlands.

Hanssen, R.F., Caro Cuenca, M., Klees, R., van der Marel, H., 2012. Decadal vertical deformation of the Netherlands via the geodetic integration of gravimetry, GNSS, leveling and SAR interferometry. In: AGU Fall Meeting Abstracts.

Heleno, S.I., Oliveira, L.G., Henriques, M.J., Falcão, A.P., Lima, J.N., Cooksley, G., Ferretti, A., Fonseca, A.M., Lobo-Ferreira, J.P., Fonseca, J.F., 2011. Persistent scatterers interferometry detects and measures ground subsidence in Lisbon. Remote Sens. Environ. 115 (8), 2152–2167.

Herrera, G., Tomás, R., López-Sánchez, J.M., Delgado, J., Mallorqui, J.J., Duque, S., Mulas, J., 2007. Advanced DInSAR analysis on mining areas: La Union case study (Murcia, SE Spain). Eng. Geol. 90 (3), 148–159.

Herrera, G., Tomás, R., Lopez-Sanchez, J.M., Delgado, J., Vicente, F., Mulas, J., Cooksley, G., Sanchez, M., Duro, J., Arnaud, A., Blanco, P., Duque, S., Mallorquí, J. J., De la Vega-Panizo, R., Monserrat, O., 2009a. Validation and comparison of advanced differential interferometry techniques: Murcia metropolitan area case study. ISPRS J. 64, 501–512.

Herrera, G., Davalillo, J.C., Mulas, J., Cooksley, G., Monserrat, O., Pancioli, V., 2009b. Mapping and monitoring geomorphological processes in mountainous areas using PSI data: central Pyrenees case study. Nat. Hazards and Earth Syst. Sci. 9 (5), 1587–1598.

Herrera, G., Notti, D., García-Davalillo, J.C., Mora, O., Cooksley, G., Sánchez, M., Arnaud, A., Crosetto, M., 2011. Analysis with C- and X-band satellite SAR data of the Portalet landslide area. Landslides 8 (2), 195–206.

Hetland, E.A., Musé, P., Simons, M., Lin, Y.N., Agram, P.S., DiCaprio, C.J., 2012. Multiscale InSAR time series (MInTS) analysis of surface deformation. J. Geophys. Res.: Solid Earth (1978–2012) 117 (B2).

Hooper, A., Zebker, H., Segall, P., Kampes, B., 2004. A new method for measuring deformation on volcanoes and other natural terrains using InSAR persistent scatterers. Geophys. Res. Lett. 31 (23).

Hooper, A., Zebker, H.A., 2007. Phase unwrapping in three dimensions with application to InSAR time series. JOSA A 24 (9), 2737–2747.

Hooper, A., 2008. A multi-temporal InSAR method incorporating both persistent scatterer and small baseline approaches. Geophys. Res. Lett. 35 (16).

Hooper, A., Pedersen, R., Sigmundsson, F., 2009. Constraints on magma intrusion at Eyjafjallajökull and Katla volcanoes in Iceland, from time series SAR interferometry. In: The VOLUME Project–Volcanoes: Understanding Subsurface Mass Movement. University College, Dublin, pp. 3–24.

Hu, J., Li, Z.W., Ding, X.L., Zhu, J.J., Zhang, L., Sun, Q., 2014. Resolving three-dimensional surface displacements from InSAR measurements: a review. Earth Sci. Rev. 133, 1–17.

Hung, W.C., Hwang, C., Chen, Y.A., Chang, C.P., Yen, J.Y., Hooper, A., Yang, C.Y., 2011. Surface deformation from persistent scatterers SAR interferometry and fusion with leveling data: a case study over the Choushui River Alluvial Fan, Taiwan. Remote Sens. Environ. 115 (4), 957–967.

Jiang, L., Lin, H., Cheng, S., 2011. Monitoring and assessing reclamation settlement in coastal areas with advanced InSAR techniques: Macao city (China) case study. Int. J. Remote Sens. 32 (13), 3565–3588.

Joughin, I.R., Kwok, R., Fahnestock, M.A., 1998. Interferometric estimation of three-dimensional ice-flow using ascending and descending passes. IEEE TGRS 36 (1), 25–37.

Jung, J., Kim, D.J., Park, S.E., 2014. Correction of atmospheric phase screen in time series InSAR using WRF model for monitoring volcanic activities. IEEE TGRS 52 (5), 2678–2689.

Kampes, B.M., Hanssen, R.F., Perski, Z., 2003. Radar interferometry with public domain tools. In: Proceedings of FRINGE 2003, Frascati, Italy.

Kampes, B.M., Hanssen, R.F., 2004. Ambiguity resolution for permanent scatterer interferometry. IEEE TGRS 42, 2446–2453.

Kampes, B.M., 2006. Radar Interferometry: Persistent Scatterer Technique. Springer, Dordrecht, The Netherlands.

Karila, K., Karjalainen, M., Hyyppä, J., Koskinen, J., Saaranen, V., Rouhiainen, P., 2013. A comparison of precise leveling and persistent scatterer SAR interferometry for building subsidence rate measurement. ISPRS Int. J. Geo-Inform. 2 (3), 797–816.

Kim, S.W., Wdowinski, S., Dixon, T.H., Amelung, F., Kim, J.W., Won, J.S., 2010. Measurements and predictions of subsidence induced by soil consolidation using persistent scatterer InSAR and a hyperbolic model. Geophys. Res. Lett. 37 (5).

Lan, H., Li, L., Liu, H., Yang, Z., 2012. Complex urban infrastructure deformation monitoring using high resolution PSI. J. Sel. Top. Appl. Earth Obs. Remote Sens. 5 (2), 643–651.

Lanari, R., Mora, O., Manunta, M., Mallorquí, J.J., Berardino, P., Sansosti, E., 2004a. A small-baseline approach for investigating deformations on full-resolution differential SAR interferograms. IEEE TGRS 42 (7), 1377–1386.

Lanari, R., Zeni, G., Manunta, M., Guarino, S., Berardino, P., Sansosti, E., 2004b. An integrated SAR/GIS approach for investigating urban deformation phenomena: a case study of the city of Naples, Italy. Int. J. Remote Sens. 25 (14), 2855–2867.

Lanari, R., Casu, F., Manzo, M., Zeni, G., Berardino, P., Manunta, M., Pepe, A., 2007a. An overview of the small baseline subset algorithm: a DInSAR technique for surface deformation analysis. Pure Appl. Geophys. 164 (4), 637–661.

Lanari, R., Casu, F., Manzo, M., Lundgren, P., 2007b. Application of the SBAS-DInSAR technique to fault creep: a case study of the Hayward fault, California. Remote Sens. Environ. 109 (1), 20–28.

Leighton, M., 2010. GPS and PSI integration for monitoring urban land motion (PhD thesis). University of Nottingham.

Liu, S., 2012. Satellite radar interferometry: estimation of the atmospheric delay (PhD thesis). Delft University of Technology.

Liu, G., Jia, H., Nie, Y., Li, T., Zhang, R., Yu, B., Li, Z., 2014a. Detecting subsidence in coastal areas by ultrashort-baseline TCPInSAR on the time series of high-resolution TerraSAR-X images. IEEE TGRS 52 (4), 1911–1923.

Liu, D., Sowter, A., Niemeier, W., 2014b. Process-related deformation monitoring by PSI using high resolution space-based SAR data: a case study in Düsseldorf, Germany. Nat. Hazards Earth Syst. Sci. Discuss. 2 (7), 4813–4830.

Lombardini, F., 2005. Differential tomography: a new framework for SAR interferometry. IEEE TGRS 43 (1), 37–44.

López-Quiroz, P., Doin, M.P., Tupin, F., Briole, P., Nicolas, J.M., 2009. Time series analysis of Mexico City subsidence constrained by radar interferometry. J. Appl. Geophys. 69 (1), 1–15.

Lundgren, P., Casu, F., Manzo, M., Pepe, A., Berardino, P., Sansosti, E., Lanari, R., 2004. Gravity and magma induced spreading of Mount Etna volcano revealed by satellite radar interferometry. Geophys. Res. Lett. 31 (4).

Lv, X., Yazici, B., Zeghal, M., Bennett, V., Abdoun, T., 2014. Joint-scatterer processing for time-series InSAR. IEEE TGRS 52 (11), 7205–7221.

Marinkovic, P., Ketelaar, G., van Leijen, F., Hanssen, R., 2007. InSAR quality control: analysis of five years of corner reflector time series. In: Proceedings of FRINGE 2007, Frascati, Italy.

Massonnet, D., Rossi, M., Carmona, C., Adragna, F., Peltzer, G., Feigl, K., Rabaute, T., 1993. The displacement field of the Landers earthquake mapped by radar interferometry. Nature 364 (6433), 138–142.

Massonnet, D., Briole, P., Arnaud, A., 1995. Deflation of Mount Etna monitored by spaceborne radar interferometry. Nature 375, 567–570.

Massonnet, D., Feigl, K.L., 1998. Radar interferometry and its application to changes in the Earth's surface. Rev. Geophys. 36 (4), 441–500.

Massonnet, D., Sigmundsson, F., 2000. Remote sensing of volcano deformation by radar interferometry from various satellites. In: Mouginis-Mark, et al. (Eds.), Remote Sensing of Active Volcanism. Geophysical Monograph, vol. 116, pp. 207–221.

Monserrat, O., Crosetto, M., Cuevas, M., Crippa, B., 2011. The thermal expansion component of Persistent Scatterer Interferometry observations. IEEE Geosci. Remote Sens. Lett. 8, 864–868.

Monserrat, O., Crosetto, M., Luzi, G., 2014. A review of ground-based SAR interferometry for deformation measurement. ISPRS J. Photogramm. Remote Sens. 93, 40–48.

Mora, O., Mallorqui, J.J., Broquetas, A., 2003. Linear and nonlinear terrain deformation maps from a reduced set of interferometric SAR images. IEEE TGRS 41 (10), 2243–2253.

Motagh, M., Hoffmann, J., Kampes, B., Baes, M., Zschau, J., 2007. Strain accumulation across the Gazikoy–Saros segment of the North Anatolian Fault inferred from Persistent Scatterer Interferometry and GPS measurements. Earth Planet. Sci. Lett. 255 (3), 432–444.

Musson, R.M., Haynes, M., Ferretti, A., 2004. Space-based tectonic modeling in subduction areas using PSInSAR. Seismol. Res. Lett. 75 (5), 598–606.

Please cite this article in press as: Crosetto, M., et al. Persistent Scatterer Interferometry: A review. ISPRS J. Photogram. Remote Sensing (2015), http://dx.doi.org/10.1016/j.isprsjprs.2015.10.011

Navarro-Sanchez, V.D., Lopez-Sanchez, J.M., 2012. Improvement of persistent-scatterer interferometry performance by means of a polarimetric optimization. IEEE Geosci. Remote Sens. Letters 9 (4), 609–613.
Navarro-Sanchez, V.D., Lopez-Sanchez, J.M., Ferro-Famil, L., 2014. Polarimetric approaches for persistent scatterers interferometry. IEEE TGRS 52 (3), 1667–1676.
Navarro-Sanchez, V.D., Lopez-Sanchez, J.M., 2014. Spatial adaptive speckle filtering driven by temporal polarimetric statistics and its application to PSI. IEEE TGRS 52 (8), 4548–4557.
Notti, D., Davalillo, J.C., Herrera, G., Mora, O., 2010. Assessment of the performance of X-band satellite radar data for landslide mapping and monitoring: upper Tena Valley case study. Nat. Hazards Earth Syst. Sci. 10, 1865–1875.
Pepe, A., Lanari, R., 2006. On the extension of the minimum cost flow algorithm for phase unwrapping of multitemporal differential SAR interferograms. IEEE TGRS 44 (9), 2374–2383.
Peltzer, G., Rosen, P., 1995. Surface displacement of the 17 May 1993 Eureka Valley, California, earthquake observed by SAR interferometry. Science 268 (5215), 1333–1336.
Pepe, A., Euillades, L.D., Manunta, M., Lanari, R., 2011. New advances of the extended minimum cost flow phase unwrapping algorithm for SBAS-DInSAR analysis at full spatial resolution. IEEE TGRS 49 (10), 4062–4079.
Perissin, D., Rocca, F., 2006. High-accuracy urban DEM using permanent scatterers. IEEE TGRS 44 (11), 3338–3347.
Perissin, D., Ferretti, A., 2007. Urban-target recognition by means of repeated spaceborne SAR images. IEEE TGRS 45 (12), 4043–4058.
Perissin, D., 2008. Validation of the submetric accuracy of vertical positioning of PSs in C-band. IEEE TGRS 5 (3), 502–506.
Perissin, D., Wang, Z., Wang, T., 2011. The SARPROZ InSAR tool for urban subsidence/manmade structure stability monitoring in China. In: Proceedings of 34th International Symposium for Remote Sensing of the Environment (ISRSE), Syndey.
Perissin, D., Wang, T., 2012. Repeat-pass SAR interferometry with partially coherent targets. IEEE TGRS 50 (1), 271–280.
Pratesi, F., Tapete, D., Terenzi, G., Del Ventisette, C., Moretti, S., 2015. Structural assessment of case study historical and modern buildings in the florentine area based on a PSI-driven seismic and hydrogeological risk analysis. In: Engineering Geology for Society and Territory – Volume 8. Springer International Publishing, pp. 345–349.
Prats-Iraola, P., Scheiber, R., Marotti, L., Wollstadt, S., Reigber, A., 2012. TOPS interferometry with TerraSAR-X. IEEE TGRS 50 (8), 3179–3188.
Quin, G., Loreaux, P., 2013. Submillimeter accuracy of multipass corner reflector monitoring by PS technique. IEEE TGRS 51 (3), 1775–1783.
Raucoules, D., Bourgine, B., De Michele, M., Le Cozannet, G., Closset, L., Bremmer, C., Veldkamp, H., Tragheim, D., Bateson, L., Crosetto, M., Agudo, M., Engdahl, M., 2009. Validation and intercomparison of Persistent Scatterers Interferometry: PSIC4 project results. J. Appl. Geophys. 68 (3), 335–347.
Reale, D., Nitti, D.O., Peduto, D., Nutricato, R., Bovenga, F., Fornaro, G., 2011. Postseismic deformation monitoring with the COSMO/SKYMED constellation. IEEE Geosci. Remote Sens. Lett. 8 (4), 696–700.
Reigber, A., Moreira, A., 2000. First demonstration of airborne SAR tomography using multibaseline L-band data. IEEE TGRS 38 (5), 2142–2152.
Righini, G., Pancioli, V., Casagli, N., 2012. Updating landslide inventory maps using Persistent Scatterer Interferometry (PSI). Int. J. Remote Sens. 33 (7), 2068–2096.
Rignot, E.J., Gogineni, S.P., Krabill, W.B., Ekholm, S., 1997. North and northeast Greenland ice discharge from satellite radar interferometry. Science 276 (5314), 934–937.
Rocca, F., 2004. Diameters of the orbital tubes in long-term interferometric SAR surveys. IEEE Geosci. Remote Sens. Lett. 1 (3), 224–227.
Rosen, P.A., Hensley, S., Joughin, I.R., Li, F.K., Madsen, S.N., Rodriguez, E., Goldstein, R. M., 2000. Synthetic aperture radar interferometry. Proc. IEEE 88 (3), 333–382.
Rosen, P.A., Hensley, S., Peltzer, G., Simons, M., 2004. Updated repeat orbit interferometry package released. Eos, Trans. Am. Geophys. Union 85 (5), 47.
Rosen, P., Lavalle, M., Pi, X., Buckley, S., Szeliga, W., Zebker, H., Gurrola, E., 2011. Techniques and tools for estimating ionospheric effects in interferometric and polarimetric SAR data. In: Proceedings of IGARSS 2011, Vancouver, pp. 1501–1504.
Rosi, A., Vannocci, P., Tofani, V., Gigli, G., Casagli, N., 2013. Landslide characterization using satellite interferometry (PSI), geotechnical investigations and numerical modelling: the case study of Ricasoli Village (Italy). Int. J. Geosci. 4 (05), 904.
Rucci, A., Ferretti, A., Monti Guarnieri, A., Rocca, F., 2012. Sentinel 1 SAR interferometry applications: the outlook for sub millimeter measurements. Remote Sens. Environ. 120, 156–163.
Samieie-Esfahany, S., Hanssen, R., van Thienen-Visser, K., Muntendam-Bos, A., 2009. On the effect of horizontal deformation on InSAR subsidence estimates. In: Proceedings of FRINGE 2009, Frascati, Italy.
Samsonov, S., Tiampo, K., 2011. Polarization phase difference analysis for selection of persistent scatterers in SAR interferometry. IEEE Geosci. Remote Sens. Lett. 8 (2), 331–335.
Sandwell, D.T., Price, E.J., 1998. Phase gradient approach to stacking interferograms. J. Geophys. Res.: Solid Earth (1978–2012) 103 (B12), 30183–30204.
Sandwell, D., Mellors, R., Tong, X., Wei, M., Wessel, P., 2011. Open radar interferometry software for mapping surface deformation. Eos, Trans. Am. Geophys. Union 92 (28), 234.
Sarabandi, K., Chiu, T.C., 1996. Optimum corner reflectors for calibration of imaging radars. IEEE Trans. Antennas Propag. 44 (10), 1348–1361.
Schmidt, D.A., Bürgmann, R., 2003. Time-dependent land uplift and subsidence in the Santa Clara valley, California, from a large interferometric synthetic aperture radar data set. J. Geophys. Res.: Solid Earth (1978–2012) 108 (B9).
Sousa, J.J., Bastos, L., 2013. Multi-temporal SAR interferometry reveals acceleration of bridge sinking before collapse. Nat. Hazards Earth Syst. Sci. 13 (3), 659–667.
Strozzi, T., Luckman, A., Murray, T., Wegmüller, U., Werner, C.L., 2002. Glacier motion estimation using SAR offset-tracking procedures. IEEE TGRS 40 (11), 2384–2391.
Strozzi, T., Teatini, P., Tosi, L., 2009. TerraSAR-X reveals the impact of the mobile barrier works on Venice coastland stability. Remote Sens. Environ. 113 (12), 2682–2688.
Tapete, D., Cigna, F., 2012. Rapid mapping and deformation analysis over cultural heritage and rural sites based on Persistent Scatterer Interferometry. Int. J. Geophys. 2012, 19p.
Teatini, P., Castelletto, N., Ferronato, M., Gambolati, G., Janna, C., Cairo, E., Marzorati, D., Colombo, D., Ferretti, A., Bagliani, A., Bottazzi, F., 2011. Geomechanical response to seasonal gas storage in depleted reservoirs: A case study in the Po River basin, Italy. J. Geophys. Res.: Earth Surf. (2003–2012) 116 (F2).
Teatini, P., Tosi, L., Strozzi, T., Carbognin, L., Cecconi, G., Rosselli, R., Libardo, S., 2012. Resolving land subsidence within the Venice Lagoon by persistent scatterer SAR interferometry. Phys. Chem. Earth, Parts A/B/C 40, 72–79.
Tofani, V., Raspini, F., Catani, F., Casagli, N., 2013. Persistent Scatterer Interferometry (PSI) technique for landslide characterization and monitoring. Remote Sens. 5 (3), 1045–1065.
Tomás, R., Cano, M., García-Barba, J., Vicente, F., Herrera, G., Lopez-Sanchez, J.M., Mallorquí, J.J., 2013. Monitoring an earthfill dam using differential SAR interferometry: La Pedrera dam, Alicante, Spain. Eng. Geol. 157, 21–32.
Torres, R., Snoeij, P., Geudtner, D., Bibby, D., Davidson, M., Attema, E., Potin, P., Rommen, B., Floury, N., Brown, M., Navas Travera, I., Deghaye, P., Duesmann, B., Rosich, B., Miranda, N., Bruno, C., L'Abbate, M., Croci, R., Pietropaolo, A., Huchlerc, M., Rostan, F., 2012. GMES Sentinel-1 mission. Remote Sens. Environ. 120, 9–24.
Vallone, P., Giammarinaro, M.S., Crosetto, M., Agudo, M., Biescas, E., 2008. Ground motion phenomena in Caltanissetta (Italy) investigated by InSAR and geological data integration. Eng. Geol. 98 (3), 144–155.
van Leijen, F., Hanssen, R., 2007. Ground water management and its consequences in Delft, the Netherlands as observed by persistent scatterer interferometry. In: Proceedings of FRINGE 2007, Frascati (Italy).
van Leijen, F., 2014. Persistent Scatterer Interferometry based on geodetic estimation theory (Doctoral dissertation). TU Delft, Delft University of Technology.
Vasco, D.W., Ferretti, A., Novali, F., 2008. Reservoir monitoring and characterization using satellite geodetic data: interferometric synthetic aperture radar observations from the Krechba field, Algeria. Geophysics 73 (6), WA113–WA122.
Vasco, D.W., Rucci, A., Ferretti, A., Novali, F., Bissell, R.C., Ringrose, P.S., Mathieson, A. S., Wright, I.W., 2010. Satellite-based measurements of surface deformation reveal fluid flow associated with the geological storage of carbon dioxide. Geophys. Res. Lett. 37 (3).
Wasowski, J., Bovenga, F., Refice, A., Nitti, D., Nutricato, R., 2015. High resolution PSI for mapping ground deformations and infrastructure instability. Engineering Geology for Society and Territory, vol. 2. Springer International Publishing, pp. 399–403.
Wegmüller, U., Walter, D., Spreckels, V., Werner, C.L., 2010. Nonuniform ground motion monitoring with TerraSAR-X persistent scatterer interferometry. IEEE TGRS 48, 895–904.
Werner, C., Wegmüller, U., Strozzi, T., Wiesmann, A., 2003. Interferometric point target analysis for deformation mapping. In: Proceedings of IGARSS 2003, Toulouse, France.
Wright, T., Parsons, B., Fielding, E., 2001. Measurement of interseismic strain accumulation across the North Anatolian Fault by satellite radar interferometry. Geophys. Res. Lett. 28 (10), 2117–2120.
Xia, Y., Kaufmann, H., Guo, X., 2002. Differential SAR interferometry using corner reflectors. In: Proceedings IGARSS 2002, Toronto.
Yu, B., Liu, G., Li, Z., Zhang, R., Jia, H., Wang, X., Cai, G., 2013. Subsidence detection by TerraSAR-X interferometry on a network of natural persistent scatterers and artificial corner reflectors. Comput. Geosci. 58, 126–136.
Zhang, L., Ding, X., Lu, Z., 2011. Ground settlement monitoring based on temporarily coherent points between two SAR acquisitions. ISPRS J. Photogramm. Remote Sens. 66 (1), 146–152.
Zhang, R., Liu, G., Li, T., Huang, L., Yu, B., Chen, Q., Li, Z., 2014. An integrated model for extracting surface deformation components by PSI time series. IEEE TGRS 11 (2), 544–548.
Zebker, H.A., Rosen, P.A., Hensley, S., 1997. Atmospheric effects in interferometric synthetic aperture radar surface deformation and topographic maps. J. Geophys. Res.: Solid Earth (1978–2012) 102 (B4), 7547–7563.
Zerbini, S., Richter, B., Rocca, F., van Dam, T., Matonti, F., 2007. A combination of space and terrestrial geodetic techniques to monitor land subsidence: case study, the Southeastern Po Plain, Italy. J. Geophys. Res.: Solid Earth 112 (B5).
Zhao, Q., Lin, H., Jiang, L., Chen, F., Cheng, S., 2009. A study of ground deformation in the Guangzhou urban area with persistent scatterer interferometry. Sensors 9 (1), 503–518.

Please cite this article in press as: Crosetto, M., et al. Persistent Scatterer Interferometry: A review. ISPRS J. Photogram. Remote Sensing (2015), http://dx.doi.org/10.1016/j.isprsjprs.2015.10.011